

High Fidelity Semantic Shape Completion for Point Clouds using Latent Optimization

Swaminathan Gurumurthy*
Carnegie Mellon University
swamig@cmu.edu

Shubham Agrawal*
Carnegie Mellon University
shubhamag@cmu.edu

Abstract

Semantic shape completion is a challenging problem in 3D computer vision where the task is to generate a complete 3D shape using a partial 3D shape as input. We propose a learning-based approach to complete incomplete 3D shapes through generative modeling and latent manifold optimization. Our algorithm works directly on point clouds. We use an autoencoder and a GAN to learn a distribution of embeddings for point clouds of object classes. An input point cloud with missing regions is first encoded to a feature vector. The representations learnt by the GAN are then used to find the best latent vector on the manifold using a combined optimization that finds a vector in the manifold of plausible vectors that is close to the original input (both in the feature space and the output space of the decoder). Experiments show that our algorithm is capable of successfully reconstructing point clouds with large missing regions with very high fidelity without having to rely on exemplar based database retrieval.

1. Introduction

With the increasing availability of low-cost RGBD scanners, the availability and consequently the need to process 3D data is becoming of great interest to the Robotics and vision community. Voxelized representations of 3D data have been quite popular in the learning community because of the ease of generalizing convolution operations to 3D. However most 3D data, whether acquired through RGBD scanners like Kinect, or through Structure-from-Motion and Stereo Cameras, or even from range scanners being incorporated into newer smartphones, is in the form of point clouds. This, along with the fact that point clouds are highly memory efficient while preserving fine surface details, makes it highly desirable to extend deep-learning methods to point clouds. Point clouds have been significantly harder to incorporate into deep learning architectures due to irregular organization

of points, i.e, they are not regular structures and can't be directly used with architectures that exploit regularity in the input for weight sharing. The networks proposed for point clouds need to be able to handle arbitrarily sized inputs and permutation in-variance.

A common challenge when reconstructing 3D scenes is that the resulting point clouds may have large missing regions. Reconstructions using Structure-from-Motion may be sparse due to lack of feature points to track on the object. Similarly the point cloud generated by a range scanner maybe have gaps due to occlusions, limited viewing angle, and be limited by the resolution of the sensor.

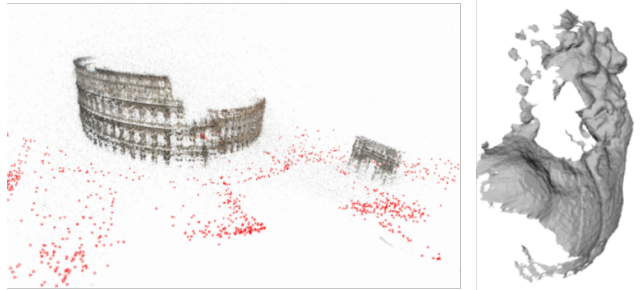


Figure 1. 3D reconstruction through techniques like Structure from Motion or RGB-D scanners often leads to incomplete shapes due to lack of feature points and occlusions respectively.

In this paper we aim to solve this challenge using a deep learning approach. We propose a framework that can take as input a point cloud with arbitrary corruption, such as large holes, entire missing regions (such as due to occlusions/viewing angle) and low resolution/ small number of points (which can also be cause by texture-less surfaces during SfM, or due to limitations in the resolution of a RGB-D sensor); and output a dense complete point cloud.

Our main contributions are as follows :

- The first shape completion framework that works directly on point clouds, and can handle all types of point cloud noises at test time such as large holes, multiple

*Both authors contributed equally

smaller missing regions, and low density, even if trained only on complete point clouds.

- A novel algorithm that performs shape completion by performing optimization on a latent manifold learnt by a generative model, using a combination of losses that ensures reconstruction of a valid object while simultaneously fitting the available data.

2. Related Work

Deep Learning on 3D data. Common tasks on point clouds include classification, segmentation, object detection and dense labeling [16, 17, 18, 19, 24]. Incorporating point clouds into a deep-learning framework poses several challenges, due to several peculiarities such as input size and order variance, non-uniform density, and shape and scaling variance.

Previously, most deep-learning approaches for point-cloud centric applications overcame these challenges by voxelizing the point clouds, which allows for the extension of ideas from 2D CNNs into the 3D space [14] [15]. However voxels are highly inefficient in terms of accuracy and fidelity of the shape represented, and the network size increases rapidly as spatial resolution is increased. More importantly, point clouds are the most common and general representation for 3D data as other representations can easily be obtained from them.

Qi et al. [1, 2] first introduced a deep learning network, PointNet, for pointcloud classification and segmentation. The network handles the arbitrary input size of point clouds by using an element wise symmetric operation, such as max-pool, to encode any input into a fixed size feature vector. This was extended in PointNet++ to use hierarchical feature learning architecture to capture both local and global geometry context.

Achlioptas et al. [5] proposed coupling a Pointnet-style encoder with a decoder of fully connected layers, along with loss metric like EMD and Chamfer distance, to learn representations of point clouds. They further showed that GMMs or GANs could be trained to directly generate the latent representations, which can be used for point cloud generation.

Another recent idea by Yu et al. [7] uses PointNet++ style encodings to capture geometric semantics of a point cloud along with feature expansion in the latent space for the task of upsampling point clouds. As noted by the authors in the paper, their approach is not suited for point clouds with large gaps or missing regions.

Shape Completion. Semantic completion of shapes with large missing areas has long been a problem of interest in the graphics and vision community. Traditional geometric methods such as by themselves can only fill in small holes in surfaces [33, 32, 31].

A lot of classical approaches relied on exemplar-based completion, where a CAD database was used to fetch similar models to reconstruct the object, which may then be deformed to match the partial input [25, 35, 34]. The vast majority of deep learning works on shape completion have relied on voxel representations due to the ease of generalizing convolution operations to 3D using 3DCNNs. Dai *et al.* used 3DCNNs to predict a coarse complete shape, which was in turn used to lookup similar model from a database. These similar models were then used together with the input for a combined complete shape synthesis. Other recent methods have removed reliance on a database by directly building predictive models for the complete 3D shape, often in a coarse-to-fine manner [27, 29, 26, 30].

The idea of using deep generative models has been shown to be effective in recovering missing regions in 2D images [11] [12]. Similar methods were extended to voxelized 3D shapes recently in [20], which incorporates a convolutional encoder-decoder, a GAN and an LSTM to better learn global and local structure.

There has been very little work done on learning-based methods for shape completion directly on point clouds. The authors of [5] show that their Autoencoder architecture may also be trained for completing point clouds. More robust formulations of the Autoencoder architecture, which incorporate neighbourhood connectivity information, have been proposed in [4, 6] although these works don't address shape completion. We note that these recently proposed approaches aimed at learning more robust representations can be seamlessly incorporated into our algorithm, as our latent-optimization is agnostic of the style of encoding-decoding mechanism used. To the best of our knowledge, we are the first to propose a deep learning based semantic shape completion approach that works directly on point clouds and can handle arbitrary corruptions in the point cloud without requiring any special training. This makes it very practical to be used in Robotics applications. We also need very small networks with much fewer parameters as compared to voxel based approaches. Our approach is purely learning based and does not rely on exemplar-based retrieval from a database, and generalizes well to objects not seen during training.

3. Methods

3.1. Generative models for point clouds

We build upon a recent model for point cloud generation proposed by Achlioptas et al. [5]. They learn an autoencoder on point clouds and then separately learn a GAN to model the distribution of feature vectors in the bottleneck layer of the autoencoder. They take inspiration from [1] to learn an autoencoder for point clouds. As in [1], the encoder consists of multiple layers of 1D convolutions followed by

a symmetric layer pooling layer (Max-Pool in this case) resulting in a single global feature vector for the entire point cloud. Because of this element wise max-pooling, the architecture can encode arbitrary sized point clouds to a fixed size feature vector. The decoder consists of a set of stacked fully connected layers. The last layer of the decoder outputs an $N \times 3$ dimensional vector which corresponds to the N points of the point cloud. They use 2 loss functions for measuring the distance between the original and the reconstructed point cloud: The EMD-distance (Equation 1) and the Chamfer-Distance (CD). Both these distance metrics are permutation invariant, which is an important property for point clouds. The EMD-Distance between two point clouds S_1, S_2 is given by:

$$d_{EMD}(S_1, S_2) = \min_{\phi: S_1 \rightarrow S_2} \sum_{x \in S_1} \|x - \phi(x)\|_2 \quad (1)$$

where $\phi : S_1 \rightarrow S_2$ is a bijection. The optimal bijection is unique and invariant under infinitesimal movement of the points. Similarly, the Chamfer-Distance between two point clouds is given by:

$$d_{CD}(S_1, S_2) = \sum_{x \in S_1} \min_{y \in S_2} \|x - y\|_2^2 + \sum_{y \in S_2} \min_{x \in S_1} \|x - y\|_2^2 \quad (2)$$

The autoencoders are trained on the ground truth complete point clouds in the training set. The trained encoder is then used to extract the global feature vector (GFV) encoding for each point cloud in the training set. The authors of [5] propose to fit a generative model on the extracted global feature vectors(GFV) and then use the decoder to generate the point cloud using the feature vectors. To this end they try two types of generative models : a Generative Adversarial Network and a Mixture of Gaussians. They observed that the distribution was simple enough that they could learn to generalize over it using a Gaussian Mixture itself. For our algorithm, we require a GAN based generative model for Point cloud completion. The Generative Adversarial Network has the advantage of being a differentiable network, it is possible to take gradients through it from the output to the input distribution space. This is key for our latent-space optimization algorithm.

Generative Adversarial Network (GAN) GAN is a popular category of generative models which has been recently shown to produce state of the art results in image generation. GANs learn a mapping from an easy to sample distribution (say, a unit normal distribution) to the data generating distribution using a function approximator like a neural network (generator). The generator(G) is trained in a game theoretic set up, where the objective of the generator is to generate samples that look indistinguishable (to another network, called the discriminator) from the data. On the other

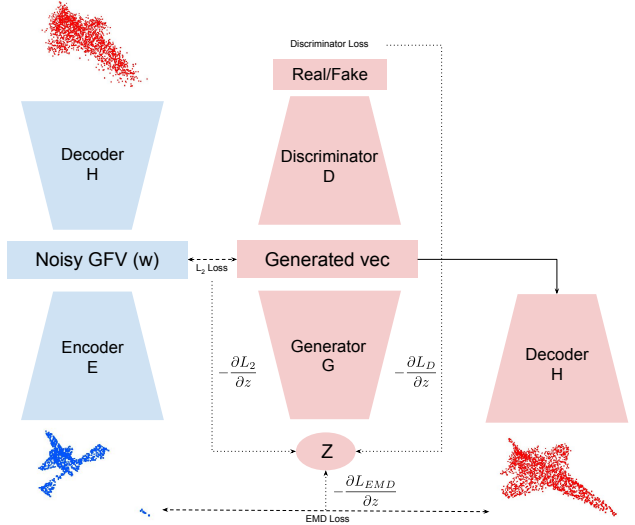


Figure 2. Point cloud completion framework

hand the discriminator (D) is trained to distinguish between the real data and the samples generated by G. Concretely, the loss functions for the generator $J^{(G)}$ and the discriminator $J^{(D)}$ can be given by:

$$J^{(D)}(\theta^{(D)}, \theta^{(G)}) = -\mathbb{E}_{x \sim p_{data}} \log D(x) - \mathbb{E}_{z \sim p_z} \log (1 - D(G(z)))$$

$$J^{(G)}(\theta^{(D)}, \theta^{(G)}) = -\mathbb{E}_{z \sim p_z} \log D(G(z))$$

where $\theta^{(D)}, \theta^{(G)}$ are the parameters for the discriminator and the generator network respectively. But this learning procedure is known to be unstable. Recent advances in GANs [22, 21, 23] have tried to address this issue by modifying the loss or the training procedure itself. We would be using one such trick proposed in [21] to modify the loss for more stable training. In our case the GAN model is trained on the global feature vectors(GFV) produced by the encoder. Since the feature vector has no structure to it, we can use a set of fully connected layers for both the Generator and the Discriminator. The architecture for the model is visualized in Figure 2 and the training procedure for the GAN is given in Algorithm 1

3.2. Point Cloud Completion using LDO

We build upon the model trained for Point cloud generation to train a generalized model for point cloud completion. Instead of directly refining the point cloud, we choose to refine the noisy global feature vector (noisy GFV) produced by the encoder using the incomplete point cloud. We then pass the refined GFV through the decoder to obtain a completed point cloud.

Thus the task is reduced to refining the noisy GFVs. We propose to do this by projecting the noisy GFV onto the

manifold of clean GFVs. This is not a trivial task since we don't have an analytical expression to represent the clean GFV manifold. Thus we use a GAN to represent the clean GFV manifold. As described in the previous section the GAN is trained on clean GFVs, extracted from the training set of complete point clouds. Projecting a noisy data point onto the clean manifold of GANs can be reduced to finding the closest GFV to the noisy GFV, that is also classified as real by the discriminator. But directly optimizing over the space of GFVs would result in adversarial examples. Thus we choose to perform the optimization procedure in the latent space of the generator. Specifically, the objective of our Latent Denoising Optimization (LDO) algorithm can be decomposed into four parts:

Discriminator Loss: This term ensures that the generated GFV is from the data manifold. We optimize to maximize the score given by the discriminator to the generated GFV:

$$L_D(z) = -\log D(G(z)) \quad (3)$$

Latent Least Squares Loss: This term ensures that the generated GFV is close to the noisy GFV during the optimization and thus remains semantically similar to the input point cloud. We simply minimize the L2 distance between the generated GFV and the noisy GFV:

$$L_2(z; w) = \|G(z) - w\|_2^2 \quad (4)$$

Decoder EMD Loss: This term ensures that the generated GFV maps to a point cloud which is close to the input point cloud where it exists. Here, we minimize the Earth Mover's distance between the input point cloud and the point cloud decoded from the generated GFV:

$$L_{EMD}(z; S_i) = d_{EMD}(S_i, H(G(z))) \quad (5)$$

Norm Loss: This term also ensures that the generated GFV is from the data manifold. We use the fact that the gaussian distribution in higher dimensions can be thought of as approximating a hollow spherical distribution with radius equal to the square root of the number of dimensions. The primary advantage of minimizing this loss is that it is much more stable than L_D and thus does not lead to spurious generations. Thus we minimize the squared error between the squared magnitude of z and the number of dimensions of z :

$$L_n(z) = [\|z\|_2^2 - N]^2 \quad (6)$$

We introduce a multi-phase optimization combining these losses to produce the completed point clouds. Specifically,

our optimization consists of 4 phases.

Phase 1: We optimize a weighted combination of L_{EMD} and L_n . Although this phase produces a blurred output with somewhat scattered point clouds, the primary objective of this phase is to produce a good initialization for the latter phases.

$$Loss(z) = L_{EMD}(z; S_i) + \alpha L_n(z) \quad (7)$$

Phase 2: The second phase consists of weighted combination of L_D and L_2 losses. The L_2 loss in this phase is given a higher weight. We include L_2 instead of L_{EMD} in this phase to ensure that the completions are semantically similar to the input point cloud. The L_D loss ensures that z doesn't go too far from the real data manifold. This phase along with Phase 1 produces a semantically meaningful and roughly overlapping point clouds which serves as a good initialization for phase 3.

$$Loss(z) = \lambda L_D(z) + \beta L_2(z; w) \quad (8)$$

Phase 3: In this phase we optimize a weighted combination of all the 4 losses mentioned above and ensures that the resulting point cloud is semantically consistent and close to the input point cloud.

$$Loss(z) = L_{EMD}(z; S_i) + \lambda L_D(z) + \beta L_2(z; w) + \alpha L_n(z) \quad (9)$$

Phase 4: In the fourth phase, we again optimize a weighted combination of L_{EMD} and L_n in order to capture the final, finer details in the input point cloud.

$$Loss(z) = L_{EMD}(z; S_i) + \alpha L_n(z) \quad (10)$$

It is important to note here that we only minimize these losses with respect to z (which is the input the Generator). We do not update the generator or discriminator parameters when performing this optimization. Thus, we obtain the corresponding vector z^* after the 4 phases of optimization. Once we obtain the optimum z^* , we simply pass it through the generator and decode the resulting GFV to obtain the completed point cloud. The entire Latent Denoising Optimization (LDO) algorithm has been given in Algorithm 2.

Algorithm 1 Training a Generative model for LDO algorithm

Require: A training set of clean, complete point clouds S .

- 1: Train an Autoencoder (with Encoder E , which may be PointNet style, and Decoder H , which can be just fully-connect layers) on the training set S , using EMD loss as the loss metric.
 - 2: Using the trained Encoder, extract the Global Feature Vectors (GFV) for all examples in the training set.
 - 3: Train a GAN to fit on the distribution of extracted GFVs from training set.
-

Algorithm 2 Point Cloud Completion using LDO algorithm

- 1: Extract the GFV w for the partial cloud S_i by passing it through Encoder E.
 - 2: Set N as total number of iterations to run the optimization
 - 3: Initialize "clean" vector z by sampling from a unit normal distribution
 - 4: **for** $i = 1, 2 \dots N/6$ **do**
 - 5: Optimize z w.r.t $L_{EMD}(z; S_i) + \alpha L_n(z)$
 - 6: **end for**
 - 7: **for** $i = 1, 2 \dots N/3$ **do**
 - 8: Optimize z w.r.t $\lambda L_D(z) + \beta L_2(z; w)$
 - 9: **end for**
 - 10: **for** $i = 1, 2 \dots N/3$ **do**
 - 11: Optimize z w.r.t $L_{EMD}(z; S_i) + \lambda L_D(z) + \beta L_2(z; w) + \alpha L_n(z)$
 - 12: **end for**
 - 13: **for** $i = 1, 2 \dots N/6$ **do**
 - 14: Optimize z w.r.t $L_{EMD}(z; S_i) + \alpha L_n(z)$
 - 15: **end for**
 - 16: Pass the cleaned GFV $G(z)$ through the previously trained Autoencoder's decoder D to obtain the semantically completed Point cloud $H(G(z))$
-

4. Experimental Results

In this section, we first describe the details of our implementation. We show the results of the baseline implementation and the corresponding point cloud generations. We then compare our model to 2 baselines on point cloud completion to demonstrate the versatility of our approach. We experiment on the ShapeNet Core [10] dataset, which is one of the most widely used dataset in the recent 3D Deep Learning literature. ShapeNetCore is a subset of the full ShapeNet dataset with single clean 3D models and manually verified category and alignment annotations. It covers 55 common object categories with about 51,300 unique 3D models. We use uniformly sampled point clouds (2048 points each) sampled from these models, which serve as the ground truth for our training. We follow a 85/5/10 train-validation-test split for our experiments and results. For the purposes of our experiments we use 4 classes with the most available data from the dataset, namely: airplane, car, chair and table.

4.1. Implementation Details

We implemented the Autoencoder as proposed by Achlioptas et al. in [5]. The encoder consists of 5 layers of 1x1 convolutions with 64, 128, 128, 256 and 128 filters respectively. Each layer is followed by a ReLU non-linearity. This is followed by a global max-pooling operation leading to a bottleneck size of 128. The decoder consists of three fully-connected layers leading to hidden layers of size 256, 256 and 6144 respectively. The output of the last layer is

reshaped to 2048×3 to get the output point cloud. The full architecture details of this AE has been described in the appendix.

The AEs were trained using an optimized approximate implementation of the the EMD/CD loss, as used by Fan et al. in [3]. From our initial results we observed that EMD metric significantly outperformed CD for the shape completion task. Hence, we have chosen EMD for our algorithm and all experiments. Similarly at test time, we use the EMD loss of the completed point clouds against the respective ground truth to evaluate our models. We use this AE to generate a set of global feature vectors for all the point clouds in the training set. We then train a W-GAN to be able to generate samples from this distribution of global feature vectors. The Generator samples from a unimodal gaussian noise distribution of 128 dimensions. It consists of two fully connected layers of size 128 each, and outputs a global feature vector of size 128. The discriminator takes a 128 dimension vector at its input. It has 2 fully connected layers of size 256 and 512 followed by a final layer which outputs one value and a sigmoid activation, resulting in a prediction of whether the input vector was real or fake. The GAN is trained with a learning rate of 0.0001 and an ADAM optimizer, for 1000 epochs.

4.2. Experiments

We compare our method against another conceivable approach, which is to train denoising autoencoders, with an augmented dataset where we feed masked point clouds at the input and train the encoder-decoder with EMD loss against the complete, ground truth point cloud at the output. While working on our experiments, we became aware that the authors of [5] updated their work to incorporate this exact baseline completion method. Thus as baseline for comparison we train these "denoising" autoencoders with varying number of points masked at the input and compare our method against them. To the best of our knowledge, we are not aware of any other learning-based method that performs semantic shape completion directly in the point cloud domain with large missing regions. Furthermore, in order to illustrate the complementary nature of our approach to the nature of autoencoder learnt, we perform latent optimization on top of denoising autoencoders also and show that there is a significant boost in performance in multiple scenarios. In the sections that follow we would be referring to the Autoencoder as AE, Denoising Autoencoder as DAE and our optimization applied on top of these approaches as LDO.

4.2.1 Varying levels of Incompletion

We train a vanilla Autoencoder (AE) using the training set in the Airplane class. We then train a Wasserstein GAN (WGAN) on the GFVs of the AE. At test time, we test the

AE and AE + LDO (Latent Denoising Optimization) with varying levels of masking (20%, 30%, 40% and 50%) in the input point cloud. The corresponding scores have been reported in Table 1. Note that we didn't have to retrain our model for the different levels of masking. We observe a clear improvement in performance using our method. We also note that the performance of AE decreases with increasing levels of masking whereas AE+LDO remains more or less robust. We also train multiple Denoising Autoencoders (DAE) along with the corresponding WGANs with varying levels of masking in the input (20%, 30%, 40% and 50%). The DAEs are trained to reconstruct the ground truth given the masked input. In this case, we test DAE and DAE + LDO with masking amounts that the DAE and the corresponding WGAN was trained on. So a DAE and WGAN trained with 40% masking are tested on 40% masking. The corresponding scores have been reported in Table 1. We observe that AE + LDO perform on par with a DAE despite not having any prior knowledge about the type or amount of incompleteness during training. Moreover, performing LDO on DAE provides further improvement as seen from the scores in Table 1. This shows that our model can integrate with any AE architecture and capitalize on the robust representations learnt by the models. A visualization of how reconstruction quality varies with increasing percentage of missing data can be found in the appendix.

4.2.2 Different classes

To show the robustness of our methods, we test our model on other classes, namely Chair, Car and Table, both in single-class and multi-class setups. We train a separate AE and the corresponding WGAN on the training set of each category. We also train separate DAEs and corresponding WGANs with 30% and 50% masking for each category. We also train a multi-class AE, WGAN pair on a training set with a combination of the four classes (Table, Chair, Car and Airplane). Correspondingly we train two DAE, WGAN pairs on the same training with 30% and 50% masking respectively (referred to as Multi-Class in results tables). We test these models on 30% and 50% masking using the corresponding test sets and report the results in Table 1. As in the previous section, the DAEs trained with specific masking amounts are tested with the same masking amounts. We observe a similar pattern as was observed in Airplane in all classes except Cars. AE+LDO performs on par or better than DAE in most of these cases. Moreover, incorporating LDO with DAE further improves the results and provides better scores than all other models in most cases. Interestingly, DAE trained on masked Cars performs better or on par with our models. On further inspection we find that this is because there is very little variety in the dataset of cars. Thus DAE is able to easily transfer from the Car training set to the Car test set by simply

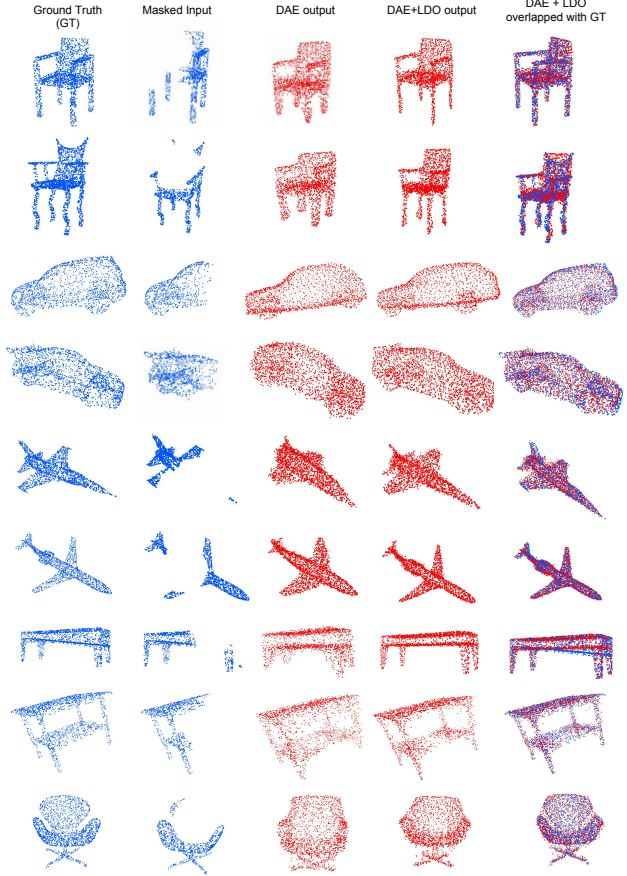


Figure 3. Visualizations of shape completions of LDO on a test set containing all 4 classes. The outputs under "DAE" are from single Denoising Autoencoder trained on objects of all 4 classes, with 50% missing data. Outputs of DAE+LDO are of the single DAE and a single WGAN trained on global feature vectors of the DAE. DAE+LDO leads to much sharper outputs with more details of the partial shape captured. Last column shows Ground truth and our results overlaid for ease of comparison.

producing the nearest neighbors from the training set. We visualize completion results with 50% masking using our best performing multi-class model (DAE + LDO) and compare it against its baseline (DAE) in Figure 3 (An enlarged version may be found in the appendix). It is seen that our multi-loss optimization ensures that both, a sharp, valid object is reconstructed, that also fits the available partial scan as best as possible. Figure 4 compares the point cloud completion results of AE and AE+LDO with 50% masking. We observe that AE produces meaningless point clouds when the inputs are very highly masked/distorted. In fact the quality of the outputs of an AE worsen with increasing levels of masking (more on this in the Appendix). Yet, just the addition of our algorithm drastically boosts the quality of results as shown in the figure.

Category	% Points Missing	AE	DAE	AE + LDO	DAE + LDO
Airplane	20%	0.061	0.033	0.029	0.028
Airplane	30%	0.079	0.036	0.042	0.033
Airplane	40%	0.083	0.039	0.041	0.033
Airplane	50%	0.097	0.039	0.039	0.037
Chair	30%	0.107	0.061	0.054	0.051
Chair	50%	0.120	0.064	0.085	0.057
Car	30%	0.096	0.0427	0.056	0.0427
Car	50%	0.118	0.046	0.061	0.054
Table	30%	0.142	0.055	0.052	0.046
Table	50%	0.143	0.055	0.063	0.050
Multi-Class	30%	0.121	0.072	0.062	0.051
Multi-Class	50%	0.113	0.069	0.059	0.052

Table 1. EMD loss of Completed point clouds against ground truth (lower is better). As baselines we compare against a Autoencoder(AE) trained only with complete point clouds as well as a Denoising AE (DAE) trained with partial point clouds. For fairness, the DAEs were trained with the same percentage of incompleteness as they were tested against. We report the performance of our LDO algorithm when used together with the AE (AE + LDO) and with the DAE(DAE+LDO). Multi-Class refers to training a single AE/DAE to reconstruct all 4 classes, as well as our own algorithm when used with these AE/DAEs

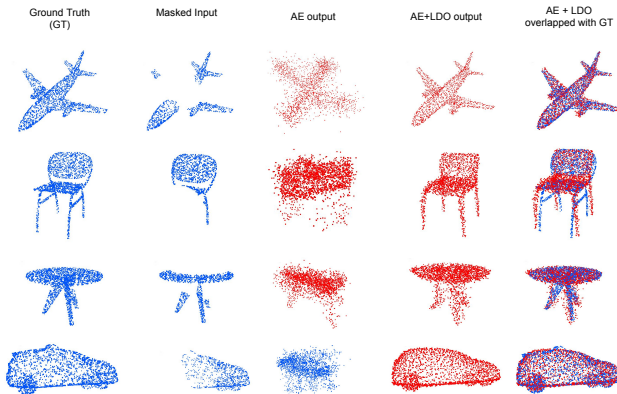


Figure 4. Visualizations of shape completion results of AE and AE+LDO on a test set containing all 4 classes. Random 50% chunks of the inputs are masked at test time. The outputs under "AE" are from a single Autoencoder trained on objects of all 4 classes. The right most column shows the AE+LDO outputs overlapped with the ground truth for direct comparison. A massive improvement is seen in reconstruction quality with our method.

4.2.3 Upsampling

Upsampling is another important task that comes up in processing 3D data. This is especially important reconstructions from Structure-from-motion methods, that often rely on sparse feature points. We investigated the performance of our algorithm for upsampling point clouds that had been downsampled to 20% points of the original, using just a regular AE without any special training, and see impressive results. We show the EMD loss for plain AE and our model in Table 2. The upsampled visualizations are given in Figure 5. We see that the Autoencoder struggles to reconstruct any

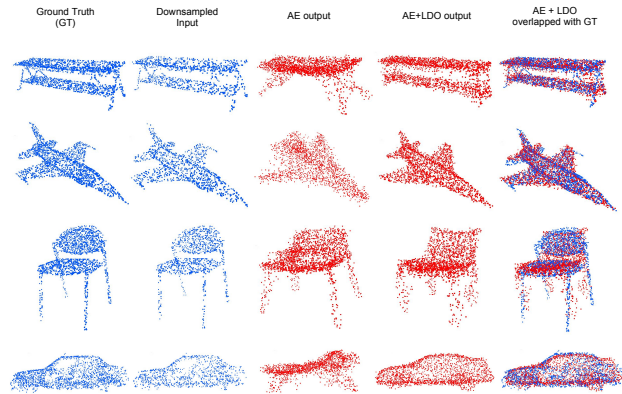


Figure 5. Visualizations of Upsampling results of AE and AE+LDO on a test set containing all 4 classes. The inputs at test time are downsampled to 1/5th of the original points. The outputs under "AE" are from a single Autoencoder trained on objects of all 4 classes. The right most column shows the AE+LDO outputs overlapped with the ground truth for direct comparison.

meaningful point clouds. Yet, just by the addition of our algorithm we observe a tremendous improvement in the up-sampling quality. The shows the versatility of our approach.

4.3. Analysis of loss functions

We show a plot of 3 losses used in LDO optimization and the EMD loss against Ground Truth (used for evaluation) during the optimization process of multi-class DAE + LDO. The plot shows that in the first phase of optimization, the Ground truth EMD Loss (EMD-GT), L2 Loss and Partial-EMD decay rapidly, whereas the Discriminator loss(LD Loss) keeps

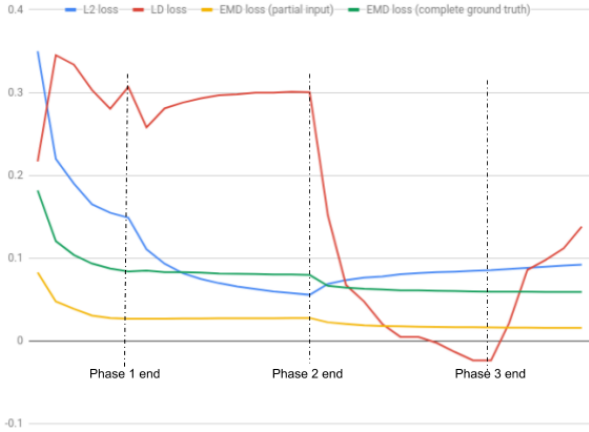


Figure 6. Plot of losses as optimization progresses. EMD loss against ground truth is used for evaluation, not for optimization.

Category	Amount of down-sampling at input	AE	AE + LDO
Multi-Class	80%	0.073	0.064

Table 2. EMD loss of Upsampled point clouds against ground truth (lower is better). As baselines we compare against a Autoencoder (AE) trained only with complete point clouds. We report the performance of our LDO algorithm when used together with the AE (AE + LDO).

oscillating. This phase was meant to provide a good initialization for further stages of optimization. In the second phase, we observe that the L2 Loss decreases rapidly but the other loss are more or less stagnant. This phase was meant to ensure that the resulting point cloud is semantically similar to the input. The third phase sees a dramatic reduction in LD Loss and a steady decay of the EMD-GT and EMD-Partial. This phase of training projects the resulting feature vector onto the real data manifold to ensure that the point cloud is coherent and similar to the data points in the training set. The fourth phase of the optimization leads to an increase in LD Loss but with a steady decrease in the EMD-GT and EMD-Partial losses. This phase captures the fine details in the point cloud and ensures that the point cloud matches with the input wherever possible.

5. Discussion and Conclusion

In this work, we presented a novel scheme for point cloud completion using a purely learning based approach. Our approach was shown to be generalizing really well to unseen objects and capable of handling a variety of different point cloud corruptions without the need for any retraining. On the other hand the denoising autoencoder had to be independently trained for the specific distortion type, and is

observed to just revert to reconstructing the nearest neighbour in the training set. Interestingly, DAE trained with a particular masking percentage performs poorly on both higher and lower masking percentages, which is highly undesirable for real-world usage (we explore this in further detail in the Appendix). Hence, while they may do well on commonly occurring objects in Shapenet, (such as airliners subclass in the airplane class, or the cars class where the vast amount of models are geometrically very similar) they fail to generalize to unseen objects. Furthermore, the denoising autoencoders don't explicitly try to match the input partial 3D structure, and thus while their output might be do well in terms of EMD loss (because the overall point distribution is roughly similar to the ground truth), the reconstructed object is clearly seen to be different than the input. The ability to generalize to unseen data despite limited training data availability (which is often the case for 3D), is a key strength of our method. Our approach allows reconstructing previously unseen objects and also is agnostic to the type of corruption. This property is especially useful when we don't have any prior knowledge about the point cloud distortion in the test set before hand. We further show that the same architecture can be used for completion of point clouds of multiple classes.

We also note that our work is agnostic of the autoencoder architecture used. Recent works have proposed more robust formulations of encoder-decoder architectures for point clouds, such as by incorporating local neighbourhood information. [2, 4, 6]. Our method can be seamlessly integrated with these enhancements along with other common autoencoder enhancements such as denoising or adversarial autoencoders. We also note that even our method misses certain fine details such as antennas in Cars and Airplanes. This is tied to the limitation of PointNet-based Autoencoder architectures, which will simply not learn to reconstruct fine structures since their penalty on the EMD loss is negligible. Thus despite our optimization against the partial scan, we cannot recover a feature vector that would lead to reconstruction of those fine details. Better Autoencoder architectures that explicitly learn to focus on fine details in point clouds are needed for this. In our future work, we would like to explore and find such architectures for point cloud based methods. In addition, we would also like to investigate other optimizers besides ADAM to see their effect on the optimization, such as possible reduction in optimization time using 2nd Order methods. We would also want to explore better strategies to initialize z , for better and faster convergence of the optimization.

Acknowledgments

We would like to thank Panos Achlioptas for sharing his implementation of the autoencoder and Haoqiang Fan for the CUDA implementation of EMD loss function.

References

- [1] Qi, C.R., Su, H., Mo, K. and Guibas, L.J., 2017. Pointnet: Deep learning on point sets for 3d classification and segmentation. Proc. Computer Vision and Pattern Recognition (CVPR), IEEE, 1(2), p.4.
- [2] Qi, C.R., Yi, L., Su, H. and Guibas, L.J., 2017. Pointnet++: Deep hierarchical feature learning on point sets in a metric space. In Advances in Neural Information Processing Systems (pp. 5105-5114).
- [3] Fan, H., Su, H. and Guibas, L.J., 2017, July. A point set generation network for 3d object reconstruction from a single image. In Conference on Computer Vision and Pattern Recognition (CVPR) (Vol. 38).
- [4] Yang, Y., Feng, C., Shen, Y. and Tian, D., 2017. FoldingNet: Interpretable Unsupervised Learning on 3D Point Clouds. arXiv preprint arXiv:1712.07262.
- [5] Achlioptas, P., Diamanti, O., Mitliagkas, I. and Guibas, L., 2017. Representation learning and adversarial generation of 3D point clouds. arXiv preprint arXiv:1707.02392.
- [6] Shen, Y., Feng, C., Yang, Y. and Tian, D., 2017. Neighbors Do Help: Deeply Exploiting Local Structures of Point Clouds. arXiv preprint arXiv:1712.06760.
- [7] Yu, L., Li, X., Fu, C.W., Cohen-Or, D. and Heng, P.A., 2018. PU-Net: Point Cloud Upsampling Network. arXiv preprint arXiv:1801.06761.
- [8] Wang, Y., Sun, Y., Liu, Z., Sarma, S.E., Bronstein, M.M. and Solomon, J.M., 2018. Dynamic Graph CNN for Learning on Point Clouds. arXiv preprint arXiv:1801.07829.
- [9] Wu, Z., Song, S., Khosla, A., Yu, F., Zhang, L., Tang, X., & Xiao, J. (2015). 3d shapenets: A deep representation for volumetric shapes. In Proceedings of the IEEE conference on computer vision and pattern recognition (pp. 1912-1920).
- [10] Chang, A. X., Funkhouser, T., Guibas, L., Hanrahan, P., Huang, Q., Li, Z., ... & Xiao, J. (2015). Shapenet: An information-rich 3d model repository. arXiv preprint arXiv:1512.03012.
- [11] Yeh, R. A., Chen, C., Lim, T. Y., Schwing, A. G., Hasegawa-Johnson, M., & Do, M. N. (2017, July). Semantic image inpainting with deep generative models. In Proceedings of the IEEE Conference on Computer Vision and Pattern Recognition (pp. 5485-5493).
- [12] Iizuka, S., Simo-Serra, E., & Ishikawa, H. (2017). Globally and locally consistent image completion. ACM Transactions on Graphics (TOG), 36(4), 107.
- [13] Rubner, Y., Tomasi, C., & Guibas, L. J. (2000). The earth mover's distance as a metric for image retrieval. International journal of computer vision, 40(2), 99-121.
- [14] Maturana, D., & Scherer, S. (2015, September). Voxnet: A 3d convolutional neural network for real-time object recognition. In Intelligent Robots and Systems (IROS), 2015 IEEE/RSJ International Conference on (pp. 922-928). IEEE.
- [15] Qi, C. R., Su, H., Nießner, M., Dai, A., Yan, M., & Guibas, L. J. (2016). Volumetric and multi-view cnns for object classification on 3d data. In Proceedings of the IEEE conference on computer vision and pattern recognition (pp. 5648-5656).
- [16] Boulch, A., Saux, B. L., & Audebert, N. (2017, April). Unstructured point cloud semantic labeling using deep segmentation networks. In Eurographics Workshop on 3D Object Retrieval (Vol. 2, p. 1).
- [17] Dohan, D., Matejek, B., & Funkhouser, T. (2015, October). Learning hierarchical semantic segmentations of lidar data. In 3D Vision (3DV), 2015 International Conference on (pp. 273-281). IEEE.
- [18] Hackel, T., Savinov, N., Ladicky, L., Wegner, J. D., Schindler, K., & Pollefeys, M. (2017). Semantic3D. net: A new large-scale point cloud classification benchmark. arXiv preprint arXiv:1704.03847.
- [19] Huang, J., & You, S. (2016, December). Point cloud labeling using 3d convolutional neural network. In Pattern Recognition (ICPR), 2016 23rd International Conference on (pp. 2670-2675). IEEE.
- [20] Wang, W., Huang, Q., You, S., Yang, C., & Neumann, U. (2017). Shape inpainting using 3d generative adversarial network and recurrent convolutional networks. arXiv preprint arXiv:1711.06375.
- [21] Arjovsky, M., Chintala, S., & Bottou, L. (2017). Wasserstein gan. arXiv preprint arXiv:1701.07875.
- [22] Goodfellow, I., Pouget-Abadie, J., Mirza, M., Xu, B., Warde-Farley, D., Ozair, S., ... & Bengio, Y. (2014). Generative adversarial nets. In Advances in neural information processing systems (pp. 2672-2680).
- [23] Mescheder, L., Nowozin, S., & Geiger, A. (2017). The numerics of gans. In Advances in Neural Information Processing Systems (pp. 1823-1833).

- [24] Li, J., Chen, B. M., & Lee, G. H. (2018, March). SO-Net: Self-Organizing Network for Point Cloud Analysis. In Proceedings of the IEEE Conference on Computer Vision and Pattern Recognition (pp. 9397-9406).
- [25] Li, D., Shao, T., Wu, H., & Zhou, K. (2017). Shape completion from a single rgb-d image. *IEEE transactions on visualization and computer graphics*, 23(7), 1809-1822.
- [26] Stutz, D., & Geiger, A. (2018). Learning 3D Shape Completion from Laser Scan Data with Weak Supervision. In Proceedings of the IEEE Conference on Computer Vision and Pattern Recognition (pp. 1955-1964).
- [27] Dai, A., Ritchie, D., Bokeloh, M., Reed, S., Sturm, J., & Nießner, M. (2018). ScanComplete: Large-Scale Scene Completion and Semantic Segmentation for 3D Scans. In CVPR (Vol. 1, p. 2).
- [28] Dai, A., Qi, C. R., & Nießner, M. (2017, July). Shape completion using 3d-encoder-predictor cnns and shape synthesis. In Proc. IEEE Conf. on Computer Vision and Pattern Recognition (CVPR) (Vol. 3).
- [29] Varley, J., DeChant, C., Richardson, A., Ruales, J., & Allen, P. (2017, September). Shape completion enabled robotic grasping. In Intelligent Robots and Systems (IROS), 2017 IEEE/RSJ International Conference on (pp. 2442-2447). IEEE.
- [30] Han, X., Li, Z., Huang, H., Kalogerakis, E., & Yu, Y. (2017, October). High-Resolution Shape Completion Using Deep Neural Networks for Global Structure and Local Geometry Inference. In Proceedings of IEEE International Conference on Computer Vision (ICCV).
- [31] Kazhdan, M., & Hoppe, H. (2013). Screened poisson surface reconstruction. *ACM Transactions on Graphics (ToG)*, 32(3), 29.
- [32] Nealen, A., Igarashi, T., Sorkine, O., & Alexa, M. (2006, November). Laplacian mesh optimization. In Proceedings of the 4th international conference on Computer graphics and interactive techniques in Australasia and Southeast Asia (pp. 381-389). ACM.
- [33] Sorkine, O., & Cohen-Or, D. (2004, June). Least-squares meshes. In Shape Modeling Applications, 2004. Proceedings (pp. 191-199). IEEE.
- [34] Li, Y., Dai, A., Guibas, L., & Nießner, M. (2015, May). Database-assisted object retrieval for real-time 3d reconstruction. In Computer Graphics Forum (Vol. 34, No. 2, pp. 435-446).
- [35] Shi, Y., Long, P., Xu, K., Huang, H., & Xiong, Y. (2016). Data-driven contextual modeling for 3d scene understanding. *Computers & Graphics*, 55, 55-67.

6. Appendix

6.1. Architecture used for Autoencoder and Denoising Autoencoder

We use the same architectures for the Autoencoder and Denoising Autoencoder. Figure 9 shows more details about the specific architecture. When feeding an incomplete point cloud we simply remove those points from the input. Since the operations performed are symmetric to all points and agnostic to the number of point clouds, the architecture works as is for incomplete point clouds as well.

6.2. DAE overfitting

We observe that the DAE overfit to the specific noise type they are trained on. If we train the DAE with a masking of 60% and test it on lower levels of masking, it's performance decreases. This can be seen in Figure 8. Taking a closer look at the completion results of the DAE, we find that the DAE has simply learnt a fixed mapping in the training set from masked clouds to the completed point clouds. When exposed to unseen data such as the test set, it simply produces a nearest neighbor from the training set. This can be seen in Figure 7.

6.3. Variation with masking

Figure 10 shows the performance of AE and AE+LDO with varying levels of masking on the Airplane category. The deterioration of performance with increasing levels of masking is clearly visible in the AE but the optimization procedure still manages to generate reasonable looking point clouds. This shows the robustness of our approach to different kinds of point cloud deformations.

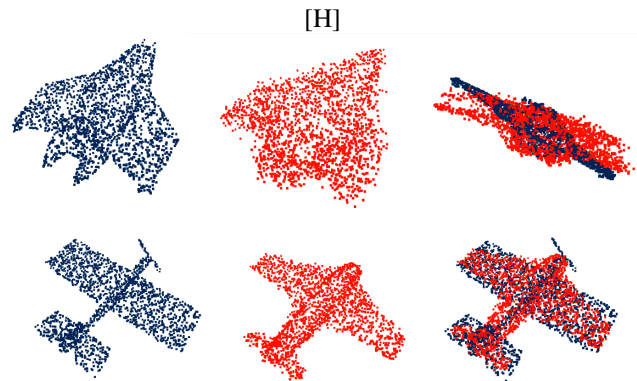


Figure 7. **DAE failure cases.** The Denoising Autoencoder is notoriously prone to overfitting on the training data. Overfitting increases with the percentage of the incompleteness with which they are trained. Column 1 has complete point clouds from the test set which were fed to the DAE without any masking. Even with a complete cloud as input, the DAE outputs a different point cloud (Column 2), since it essentially collapses to a Nearest Neighbour search against the training data. The difference between input and DAE output is visualized in column 3. Due to lack of large datasets for 3D, this is a huge disadvantage of the plain DAE. We also note in our experiments that a DAE trained with higher percentages of missing data performs poorly on lower percentages of corruption.

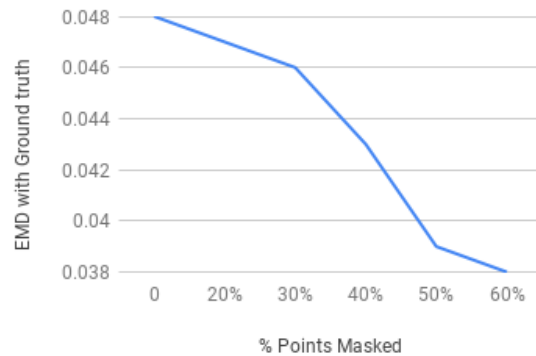


Figure 8. The plot shows the performance of Denoising Autoencoder (trained on point clouds with 60% masking) with different levels of masking. The plot shows that the DAE performs worse as the masking is reduced. Infact, it gives the worst performance when the ground truth (0% masking) is given as input.

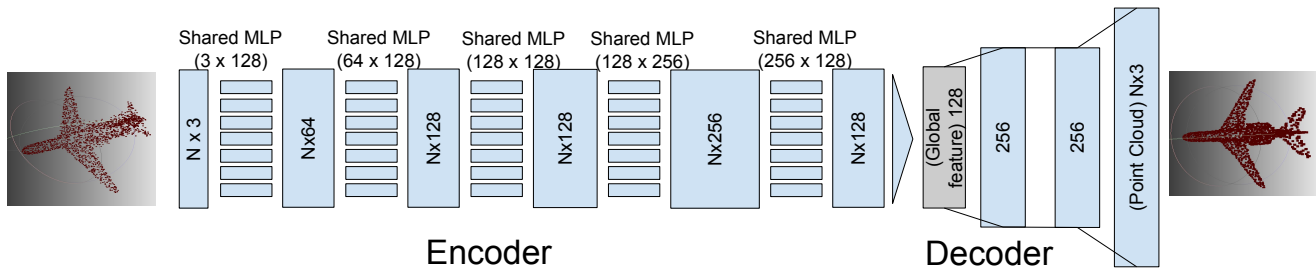


Figure 9. Autoencoder Architecture.

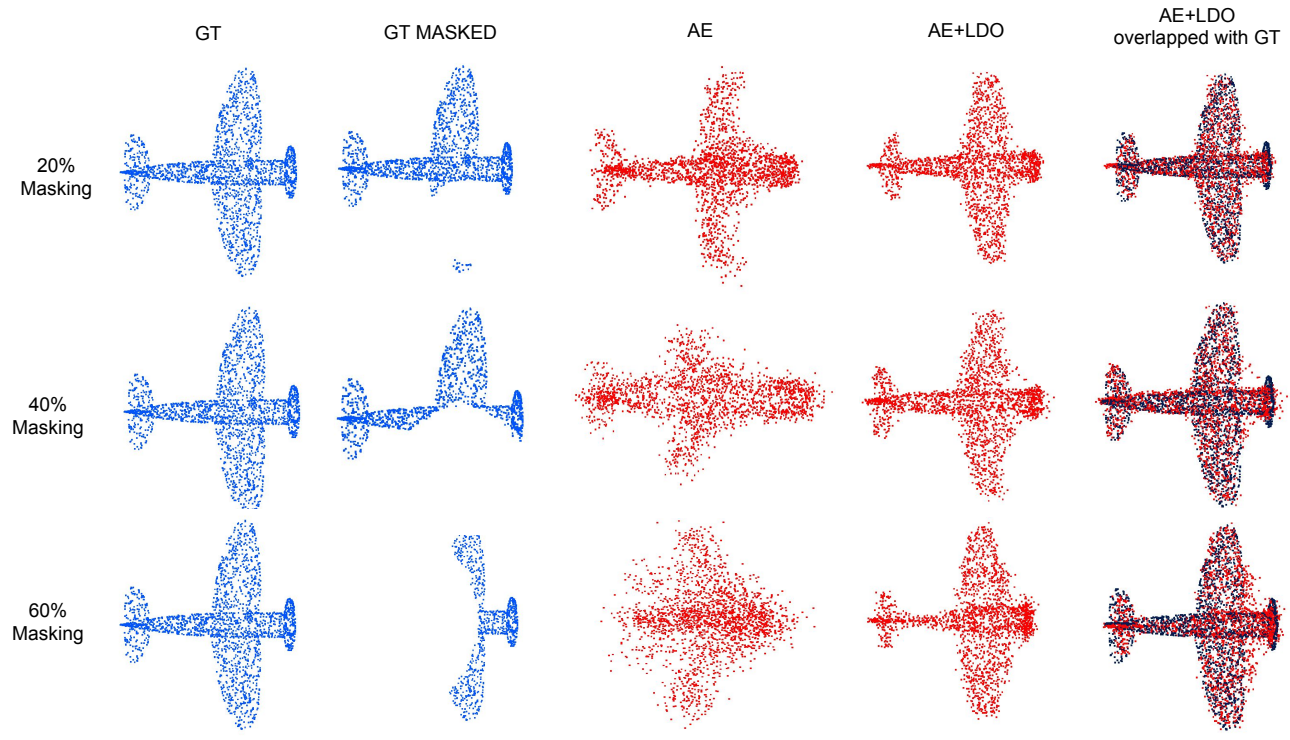


Figure 10. The figure shows the performance of AE and AE+LDO with varying levels of masking (20%, 40% and 60%). The AE in this case is trained specifically on the Airplane dataset.

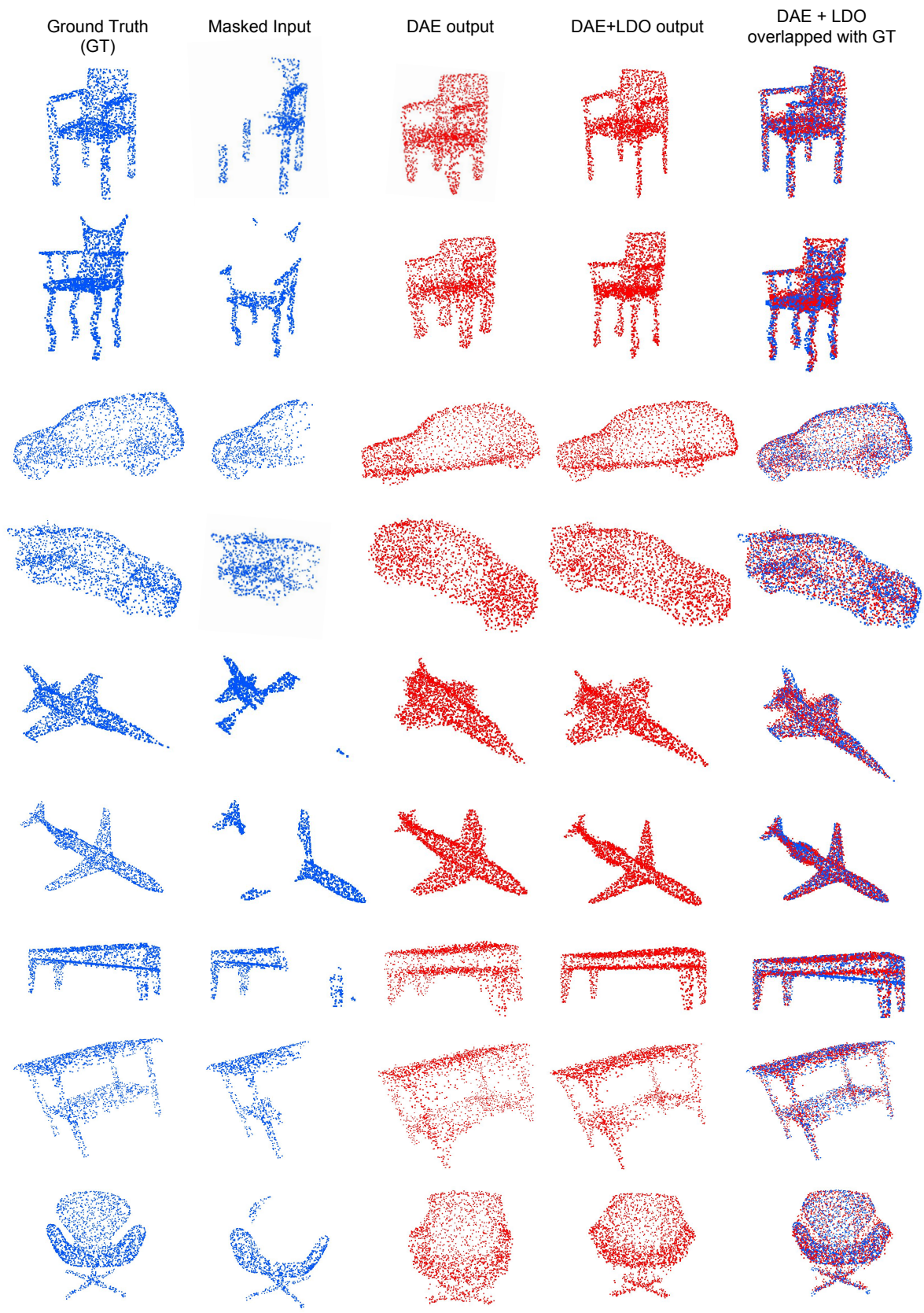


Figure 11. Enlarged version of Fig. 3 results in main paper, showing reconstructions of Multi-Class DAE and Multi-Class DAE+LDO